Nano Research 2017, 10(12): 4210–4220
DOI 10.1007/s12274-017-1662-8
Research Article
ISSN 1998-0124
CN 11-5974/O4

Simultaneous surface modification method for $0.4Li_2MnO_3$-$0.6LiNi_{1/3}Co_{1/3}Mn_{1/3}O_2$ cathode material for lithium ion batteries: Acid treatment and $LiCoPO_4$ coating

Min-Joon Lee, Eunsol Lho, Pilgun Oh, Yoonkook Son, and Jaephil Cho (✉)

Department of Energy Engineering, School of Energy and Chemical Engineering, Ulsan National Institute of Science and Technology (UNIST), Ulsan 44919, Republic of Korea

Received: 13 February 2017
Revised: 8 April 2017
Accepted: 29 April 2017

© Tsinghua University Press and Springer-Verlag Berlin Heidelberg 2017

KEYWORDS
lithium ion battery,
cathode material,
Li-rich material,
electrochemistry,
surface modification

ABSTRACT

Li-rich layered cathode materials have been considered the most promising candidates for large-scale Li-ion batteries due to their low cost and high reversible capacity. However, these materials have many drawbacks that hinder commercialization, such as low initial efficiency and cyclability at elevated temperatures. To overcome these barriers, we propose an efficient and effective surface modification method, in which chemical activation (acid treatment) and $LiCoPO_4$ coating were carried out simultaneously. During the synthesis, the lithium ions were extracted from the lattice, leading to improved Columbic efficiency, and these ions were used for the formation of $LiCoPO_4$. The Ni and Co doped spinel phase was formed at the surface of the host material, which gives rise to the facile pathway for lithium ions. The $LiCoPO_4$ and highly doped spinel on the surface acted as double protection layers that effectively prevented side reactions on the surface at 60 ˚C. Moreover, the transition metal migration of the modified cathode was weakened, due to the presence of the spinel structure at the surface. Consequently, the newly developed Li-rich cathode material exhibited a high 1st efficiency of 94%, improved capacity retention of 82% during 100 cycles at 60 ˚C, and superior rate capability of 62% at 12C (1C = 200 mA/g) rate at 24 ˚C. In addition, the thermal stability of the modified cathode was significantly improved as compared to that of a bare counterpart at 4.6 V, showing a 60% decrease in the total heat generation.

1 Introduction

Lithium ion batteries (LIBs) are attracting considerable attention as the most promising energy storage systems for electric vehicles (EVs) as well as small portable devices, because of their advantages, including low self-discharge rate, high energy density, and long cycle life. EVs equipped with small-sized LIBs and motors,

Address correspondence to jpcho@unist.ac.kr

which are called hybrid electric vehicles (HEVs), achieve better fuel economy. HEVs mainly use spinel $LiMn_{2-x}M_xO_4$ (M = Li, Al, Mg, Co, etc.) as the cathode material to fulfill the power and durability requirements of HEVs. However, in the EV mode, their driving range can be very short because small-sized LIBs are mainly composed of spinel cathode materials with low energy density [1–3].

With the rapid increase in the need for EVs with higher mileage, extensive and intensive research has been carried out on possible cathode materials with higher energy density than that of spinel cathode materials. These include Li-rich layered materials Li_2MnO_3-$LiMO_2$ (M = Ni, Co, Mn, Cr, Fe, etc.) [4–6] and Ni-rich layered materials $LiNi_{1-x}M_xO_2$ ($1 - x > 0.6$; M = Co, Mn, Al, etc.) [7–9]. Among them, the Li-rich layered materials have attracted considerable interest because of their higher specific capacity (> 240 mAh/g between 2.0 and 4.6 V) and lower cost. However, they have several drawbacks such as low Coulombic efficiency in the 1st cycle, voltage decay with cycling, intrinsically poor rate capability, and irreversible side reactions with the electrolyte due to the high cut-off voltage, especially at elevated temperatures (> 60 ˚C) [10–13]. In order to overcome such problems, many solutions have been proposed. Surface coating using inert ceramics such as metal oxides, fluorides, and phosphates (Fig. 1(a)) is frequently investigated for improvement of the electrochemical performance [4, 14–18]. These coating materials act as a protective layer against the acidic electrolyte, resulting in a decrease in side reactions on the surface. Another approach to overcome the drawbacks is an acid treatment for chemical activation, which is intended to improve the initial efficiency [19–21]. In this process, lithium ions are extracted from the lattice via an H^+/Li^+ exchange reaction. However, it is believed that the extracted lithium ions could be converted into lithium impurities such as Li_2CO_3 and LiOH, which cause gas evolution during the 1st charge, unless fully removed (Fig. 1(b) and Fig. S1 in the Electronic Supplementary Material (ESM)). Recently, our group proposed a reduced graphene oxide (RGO)-coated Li-rich material. Graphene oxide (GO) was reduced by hydrazine treatment, and a material with submicron-sized flake-shaped primary particles was obtained [22, 23]. Both studies showed significant improvements in performance. However, no investigation has been conducted at elevated temperatures, even though cell evaluations at an elevated temperature (> 60 ˚C) are very critical because LIBs are usually packed in a closed space causing heat accumulation. In addition, the safety

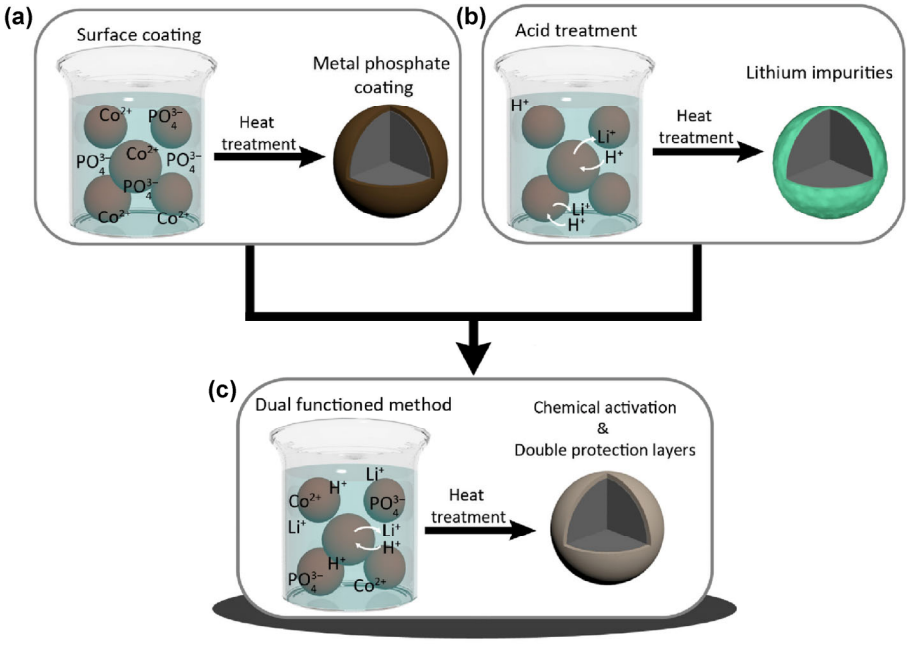

Figure 1 Schematic view of the fabrication processes and their final results for (a) surface coating, (b) acid treatment, and (c) dual functioned method.

issues should be considered. Other groups have reported many investigations on the surface coating and acid treatment of Li-rich cathode materials to overcome their electrochemical and thermal weaknesses [4, 14–21]. For instance, Su Y. F. et al. reported a spinel membrane-encapsulated Li-rich material [24]. The cells had outputs between 2.0 and 4.8 V, and showed improved electrochemical performances such as rate capability, Coulombic efficiency, and cyclability; however, no investigation of cycling performance at an elevated temperature (> 60 ℃) was mentioned. The PNNL group found that a possible origin of the voltage decay was the uneven distribution of Ni elements in the cathode, and that one way to minimize the voltage decay at room temperature was the hydrothermal method, which led to uniform distribution of Ni elements [5, 25, 26].

Apart from the inherent voltage decay due to the spinel-like phase transition during a cycle, other critical test criteria, such as gas evolution from the Li impurities on the cathode surface due to acid treatment, rate capability, 1st Coulombic efficiency, cycling performance at elevated temperature, and thermal instability, have never been addressed at the same time. Therefore, it is necessary that efficient and effective methods, which can carry out surface coating and acid treatment for chemical activation simultaneously, should be developed to overcome such drawbacks. In addition, the candidate coating material should react with residual impurities to eliminate side reactions [27, 28].

Herein, we report the $LiCoPO_4$ coated $0.4Li_2MnO_3$-$0.6LiNi_{1/3}Co_{1/3}Mn_{1/3}O_2$, synthesized by the efficient dual-functioned coating method (Fig. 1(c)). The lithium ions in the coating material $LiCoPO_4$ originated from the host material, when it was stirred in an acidic solution with cobalt and phosphate ions. During heating process, these ions were consumed to form $LiCoPO_4$ on the surface of the host particles. In addition, the structure from which the lithium ions were extracted, recrystallized to form the spinel surface layers. The two protection layers on the surface (Ni and Co doped spinel and $LiCoPO_4$) effectively suppressed the side reactions leading to an improved electrochemical performance compared with the bare $0.4Li_2MnO_3$-$0.6LiNi_{1/3}Co_{1/3}Mn_{1/3}O_2$. More importantly, the coated cathode demonstrated considerably less heat evolution at 4.6 V, compared with the bare counterpart.

2 Experimental

2.1 Synthetic method

To begin, the $Ni_{0.2}Co_{0.2}Mn_{0.6}(OH)_2$ powder was synthesized via co-precipitation method. Stoichiometric amounts of $NiSO_4·6H_2O$, $CoSO_4·6H_2O$, and $MnSO_4·5H_2O$ were used as the starting materials. An aqueous solution (Ni:Co:Mn = 0.2:0.2:0.6 in molar ratio) at a concentration of 2.0 $mol·L^{-1}$ was pumped into a continuously stirred tank reactor (CSTR, 4 L) in a nitrogen atmosphere. The pH was adjusted to 10.5 with NaOH solution of 4.0 $mol·L^{-1}$, and a certain amount of NH_4OH solution was separately fed into the reactor as a chelating agent. The resulting powder was filtered and washed many times with distilled water, and then dried at 110 ℃ for 12 h. The dried powder was thoroughly mixed with LiOH at a molar ratio of 1:1.44 and calcined at 900 ℃ for 10 h to obtain $0.4Li_2MnO_3$-$0.6LiNi_{1/3}Co_{1/3}Mn_{1/3}O_2$ (bare). To prepare the coated sample, the bare powder was immersed into an acidic solution of $Co(NO_3)_2·6H_2O$ and H_3PO_4 (85 wt.% in H_2O) for chemical activation. The mixture was stirred vigorously at 150 ℃ until the water was removed, and then the resulting powder was heated at 600 ℃ for 3 h.

2.2 Characterization

The crystal structure was confirmed by a powder X-ray diffractometer (XRD, D/Max-2200 V, Rigaku) using Cu Kα radiation. The morphologies of the prepared samples were examined using scanning electron microscopy (SEM, S-4800, HITACHI). The samples for transmission electron microscopy analysis were prepared using focused ion beam (FIB, Quanta 3D FEG, FEI). To analyze the structure on an atomic scale, high-resolution transmission electron microscopy (HR-TEM, JEM-2100F, JEOL), operated at 200 kV, was used. For the differential scanning calorimetry (DSC) analysis, CR2032 coin-type cells were fully charged at 4.6 V and opened carefully in a dry room. After the current collectors were washed with dimethyl carbonate (DMC) and dried, the sample, along with 30 wt.%

electrolyte, was sealed inside stainless steel high-pressure capsules to prevent leakage of the pressurized solvents. The DSC curves were measured from 50 to 350 ℃ at a scan rate of 5 ℃·min^{-1}.

2.3 Electrochemical measurements

The cathode electrodes were fabricated by blending the prepared powders (85 wt.%), Super P carbon black (5 wt.%), and polyvinylidene fluoride (10 wt.%). Galvanostatic charge-discharge cycling was carried out using CR2032 coin-type cell, which consists of a cathode and a lithium metal anode separated by porous polypropylene film, assembled in an argon-filled glove box. The electrolyte solution was 1.15 M $LiPF_6$ in mixture of ethylene carbonate (EC) and ethyl methyl carbonate (EMC) in 3:7 volume ratio (PANAX ETEC Co. Ltd., Korea). All the electrochemical tests were performed on WBCS-3000 (WonATech Co.). The galvanostatic charge-discharge tests were conducted in a voltage range of 4.6 to 2.0 V vs. Li/Li$^+$. The active material loading was 4 mg/cm. Electrochemical impedance spectroscopy (EIS) was performed for a frequency range of 0.02 to 250 kHz using an electrochemical interface system (IVIUM) on coin-type half cells at 4.6 V.

3 Results and discussion

In order to confirm the crystal structure of the prepared samples, the XRD measurement was carried out, and its results are shown in Fig. S2 in the ESM. The XRD patterns of the bare $0.4Li_2MnO_3$-$0.6LiNi_{1/3}Co_{1/3}Mn_{1/3}O_2$ (denoted as bare) indicate typical Li_2MnO_3-$LiMO_2$ composite phases [4, 19]. Weak super-lattice reflection peaks appeared between 20° and 25°. The 2 wt.% $LiCoPO_4$ coated sample (denoted as 2LCP) has similar peaks with the bare and almost indiscernible impurity peaks can be seen. The peak intensities of this impurity increased when the coating was increased to 5 wt.% (denoted as 5LCP). The amount of impurity is in good agreement with that of the olivine $LiCoPO_4$ of space group *Pnma*. From these results, it is reasonable to infer that the lithium ions were extracted through H^+/Li^+ exchange reaction when the material was stirred in the acidic solution, and that $LiCoPO_4$ was successfully formed with the extracted lithium ions and the cobalt and phosphate ions that were introduced when it was heated further.

The morphologies of the bare and 2LCP powders were confirmed by the SEM. As seen in Figs. S3(a) and S3(b) in the ESM, no significant change in morphology can be observed after coating. Moreover, the evenly distributed phosphorous ions demonstrate that the $LiCoPO_4$ was well coated on the surface of the bare, according to the energy dispersed X-ray (EDX) analysis (Figs. S3(c)–S3(f) in the ESM). The X-ray photoelectron spectroscopy (XPS) profile for C 1s showed no carbon peak for Li_2CO_3, which indicates that the extracted lithium ions were well consumed to form $LiCoPO_4$ on the surface (Fig. S5 in the ESM).

To analyze the microstructures of the samples on an atomic scale, measurements were carried out using scanning transmission electron microscopy (STEM). Figures 2(a) and 2(c) show high-angle annular dark-field (HAADF) STEM images of the cross sections of bare and 2LCP, respectively. No coating layers are observed on the surface of the bare particle (Fig. 2(a) and Fig. S4(a) in the ESM). However, in the case of the coated sample, rough coating layers can be found on the host material, which appears to be an amorphous phase (Fig. 2(c) and Fig. S4(b) in the ESM). It is revealed that the layered structure ($R\bar{3}m$) is based on the cubic close packed (ccp) oxygen arrangement, while the olivine structure (*Pnma*) has the hexagonal close packing (hcp) array of oxygen ions. Moreover, the transition metal and lithium ion sites are dependent on the oxygen framework. Therefore, when the zone axis is focused on the layered host material, the olivine coating material looks like an amorphous phase, and appears unclear due to the different oxygen array. The atomic distribution of this coating layer was confirmed by the EDX analysis (Figs. 2(e)–2(h)). As can be seen, the cobalt and phosphorus atoms were evenly distributed on the host material. From the EDX results and the XRD patterns, it is concluded that olivine $LiCoPO_4$ coating layer was successfully formed on the surface. The coating method introduced in this study, combined with the acid treatment (chemical activation), leads to structural changes. Figures 2(b) and 2(d) show the magnified images of Figs. 2(a) (bare) and 2(c) (2LCP), respectively. The crystal structure

of bare corresponds to the layered structure ($R\bar{3}m$) when the viewing direction is $[010]_{trigonal}$, and a thin NiO layer was observed on the outermost surface. Interestingly, after the surface modification, the surface structure of 2LCP was obviously changed to spinel (inner) and spinel-like (outer) phases (Fig. 2(d)) [29, 30]; the spinel phase has a diamond configuration with eight Mn columns (Fig. 2(j)) along the $[110]_{cubic}$ zone axis and the spinel-like phase has a weak contrast in the center of the Mn diamond. It was reported that the structure of Li-rich materials is continuously changed from layered to spinel during the electrochemical cycling, and the spinel-like phase is considered as a medium state between layered and spinel structures [22]. When the lithium ions are extracted, the transition metal ions migrate to the empty lithium sites, leading to the formation of the spinel phase, and finally the rock salt NiO phase appears. In this study, the spinel phase was clearly observed. The reason for this is believed to be as follows. When the bare materials were immersed in the acidic solution, in which the coating precursors were dissolved, the lithium ions were extracted from the lattice at the surface and a lithium deficient phase was formed. Accordingly, after the heat treatment, the structures of the surface were transformed into the spinel phase, which is

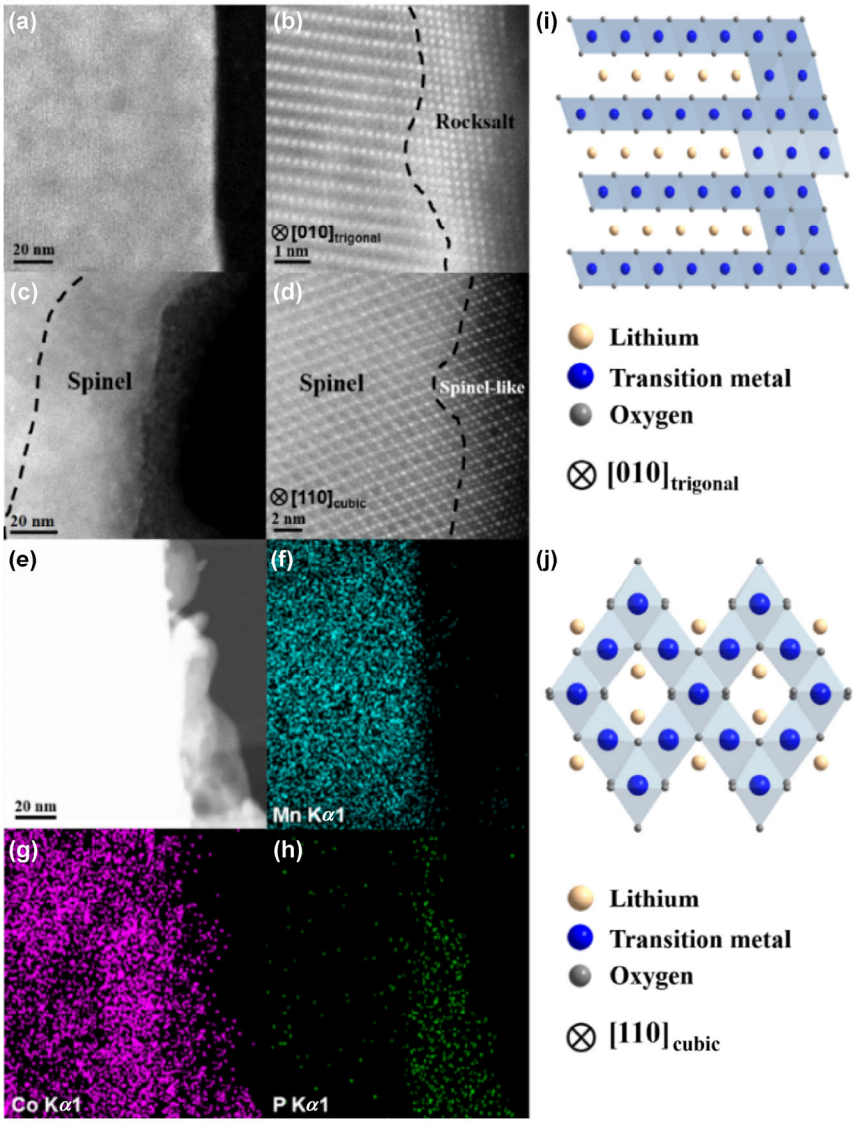

Figure 2 (a) STEM image of bare, (b) magnified image of (a), (c) STEM image of 2LCP, (d) magnified image of (c), (e)–(h) EDX mapping results of 2LCP, structural schematic diagrams of (i) layered structure with cation-disorder surface and (j) spinel structure.

thermodynamically more stable. The atomic distributions of the bare and 2LCP samples were confirmed by the EDX analysis (Fig. 3). In the case of the bare, the atomic ratios of Ni, Co, and Mn are approximately 20%, 20%, and 60%, respectively, as synthesized (Figs. 3(a) and 3(d)). The outermost surface showed slightly higher Ni composition due to the small amount of cation disorder (NiO). However, the transition metal distribution of the surface is fully changed after coating. As can be seen in Fig. 3(b) and €, the concentrations of Ni and Mn are deficient, while that of Co is rich, compared to the bare. However, in the case of the inner part, the content of Mn is steeply increased, while that of Co is decreased (Figs. 3(c) and 3(f)). The composition of region 2 in Figs. 3(c) and 3(f) is almost similar to that of the bare. Consequently, it is reasonable to deduce that, during the heating process, the Co ions preferentially moved to empty lithium sites at the surface region, which resulted in the formation of spinel structure at the inner surface and spinel-like phase at the outer surface.

Figure 4(a) shows the initial charge and discharge curves of the bare and 2LCP electrodes between 2.0 and 4.6 V at 0.1C rate (1C = 200 mA/g) at 24 ℃. The bare electrode delivered a relatively higher charge capacity of 280 mAh/g, while the 2LCP electrode showed a lower charge capacity of 270 mAh/g. The reason for this is believed to be that the lithium ions are extracted from the lattice of Li_2MnO_3 during the coating process, leading to reduced charge capacity above 4.4 V [4, 19, 31]. The discharge capacity decreased slightly, which could be due to the reduced portion of active materials. As a result, the Coulombic efficiency was improved after the surface modification. In addition,

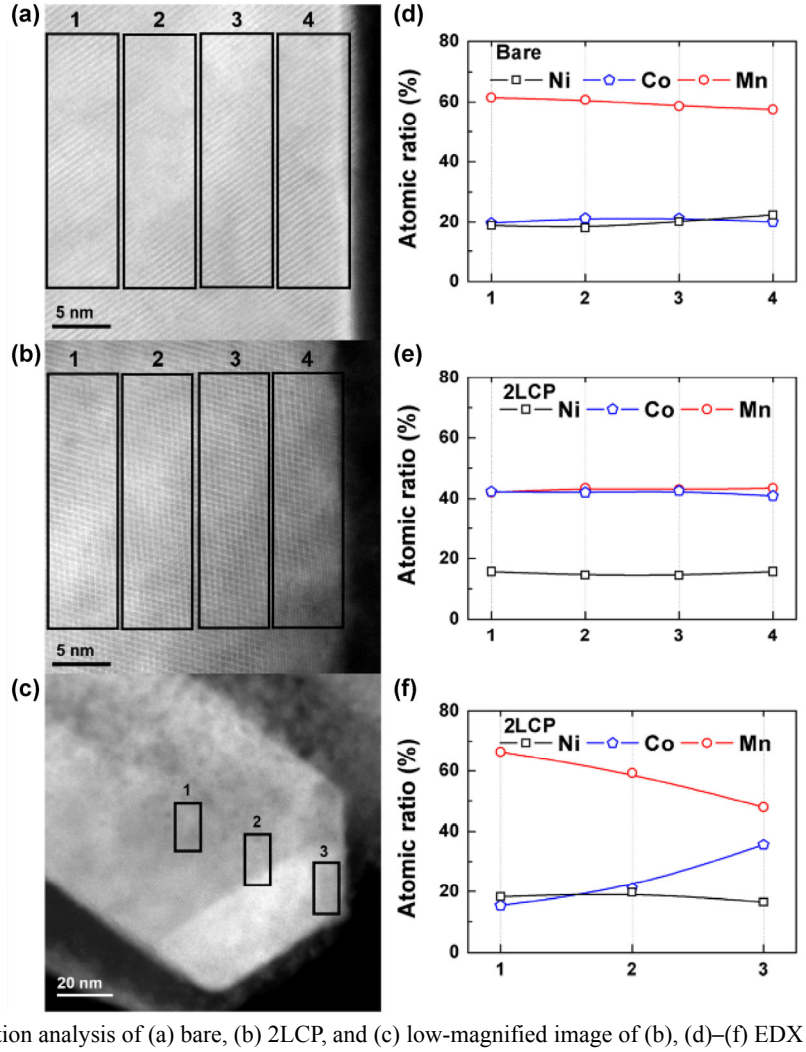

Figure 3 EDX composition analysis of (a) bare, (b) 2LCP, and (c) low-magnified image of (b), (d)–(f) EDX mapping results.

unknown plateaus were found near 2.55 V for the 2LCP electrode. From the STEM analysis, this is considered to be the spinel 2.8 V plateau. However, no investigation was carried out in this study to find out why it showed a lower potential than in other reports [4, 32]. Figure 4(b) shows the capacity retentions of the bare and 2LCP electrodes as a function of various C rates from 0.5C to 12C at 24 ˚C. The charge rate was fixed at 0.5C rate. It is obvious that the rate capability of the 2LCP electrode was higher than that of the bare. For example, the discharge capacity retention of the 2LCP electrode at 12C was 62.0% (135 mAh/g) of its discharge capacity at 0.5C rate, while that of the bare electrode was 49.2% (107 mAh/g). The improved rate capability can be explained by the higher lithium diffusion coefficients (D_{Li^+}), which were determined using the Warburg impedance in the low frequency region (Fig. 5). The D_{Li^+} of 2LCP is 6.92×10^{-10} cm^2/S (Warburg constant, σ = 2.002), while that of bare is 1.02×10^{-10} cm^2/S (σ = 0.769). In addition, the reduced total impedance affected the properties of fast charge and discharge (Fig. 5). The improved D_{Li^+} and reduced resistance are related to the presence of spinel phase on the surface of Li-rich materials. It gives rise to enhanced electrochemical performances, because the 3D structure of spinel provides more facile pathway for lithium ions [24, 33]. Figure 4(c) shows the continuous cycling results of the bare and 2LCP electrodes at 24 ˚C, when the charge and discharge current densities were maintained at 1C rate. The capacity retention and working voltages of 2LCP were improved slightly, compared to that of bare at 24 ˚C (Figs. 4(c), 4(d), and Fig. S6 in the ESM); the working voltage was obtained from the midpoint potential of the discharge curves in this study. These trends of cycling performances were completely changed when the evaluations were carried out at an accelerated test condition (60 ˚C). As can be seen in Figs. 4(e), 4(f), and Fig. S7 in the ESM,

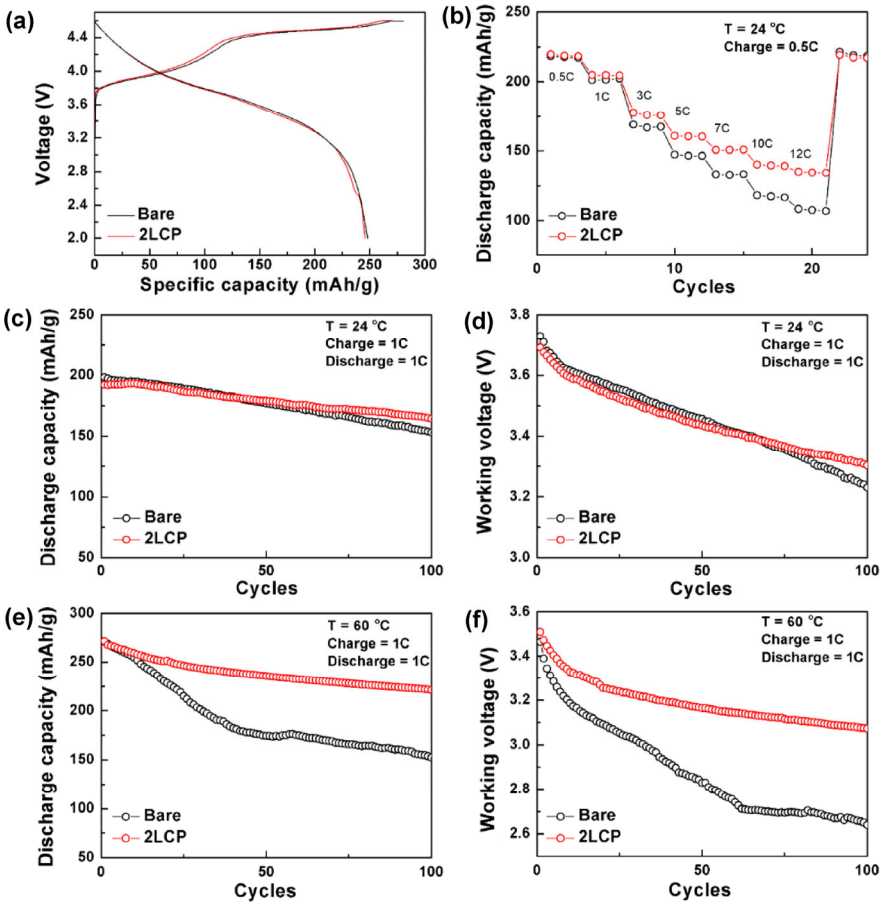

Figure 4 (a) First charge-discharge curves, (b) discharge capacity retention as a function of various C rates from 0.5C to 12C. (c) Continuous cycling results at 24 ˚C and (d) its working voltages. (e) Continuous cycling results at 60 ˚C and (f) its working voltages.

the difference of cycling and working voltage retentions between the bare and 2LCP electrodes at 60 ℃ became bigger than at 24 ℃, due to the higher reactivity between the surface of the electrode materials and the acidic electrolyte. The bare electrode exhibited significant capacity fading due to the dissolution of the transition metal and the increased surface resistance resulting from the byproducts on the surface, while the 2LCP electrode exhibited much improved cycling performance (Fig. S8 in the ESM). It is well known that the mechanisms of voltage decay in Li-rich layered materials come from the structural change in bulk, and that the side reaction on the surface results in large polarization. In previous papers, it was reported that the spinel phase at the surface reduces voltage decay [4, 24]. In our study, the artificially induced spinel structure might partly prevent the transition metal migration to the lithium layers, because half of the lithium slabs were already occupied by cations to form the spinel structure, leading to the alleviated voltage decay at both 24 and 60 ℃. Moreover, the two protection layers, Ni and Co doped spinel and $LiCoPO_4$ structures, effectively reduced the side reactions on the surface. This result is in good agreement with the EIS results.

Figure 5 shows the typical Nyquist plots for the bare and 2LCP samples after every 25 cycles at 60 ℃. Even though it was very difficult to deconvolute each of the surface film (R_{sf}) and charge-transfer resistance (R_{ct}) values from the overlapped semicircles in this study, the total impedance of the bare electrode significantly increased to more than that of the 2LCP electrode with increasing cycle numbers. From this, it can be certain that harsher side reactions occurred on the surface of the bare electrode, leading to worse cycling performance and severer voltage decay.

For commercialization, the safety issues of cathode materials should be considered, because it directly affects the safety of the battery. To evaluate the thermal stability, DSC analysis was carried out. Figure 6(a) shows the DSC measurement results of the bare and 2LCP electrodes charged to 4.6 V in the presence of the electrolyte. The main peak of 2LCP at 259 ℃ is higher than that of bare at 240 ℃. Moreover, the 2LCP electrode generated significantly lower heat (398 J/g) than the bare electrode (985 J/g). The improved thermal

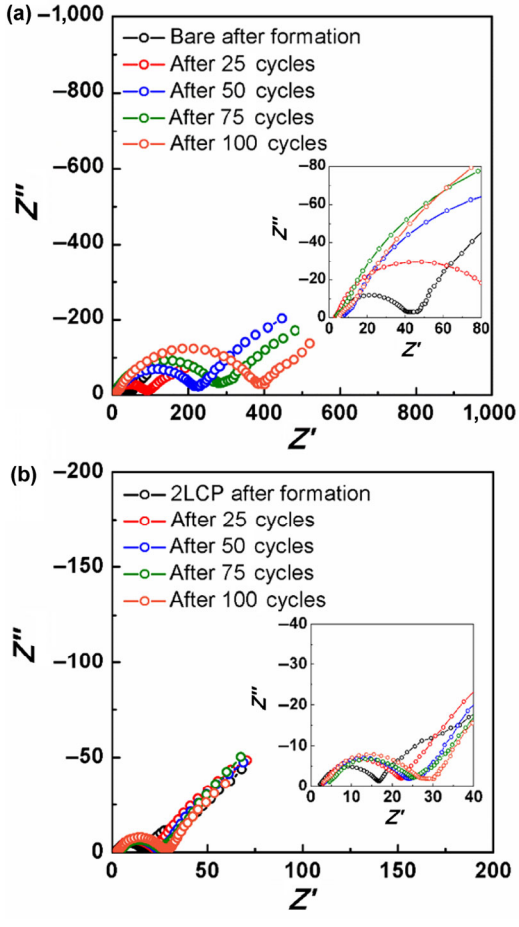

Figure 5 Nyquist plot for (a) bare, and (b) 2LCP with respect to cycle number: 1st, 25th, 50th, 75th, 100th cycles.

property is ascribed to the double protection of cation-doped spinel and $LiCoPO_4$ layers, which have a relatively good thermal stability, because those materials are not fully delithiated when charged to 4.6 V [34–37], resulting in less structural instability. These stable layers protect the cathode surface from being directly exposed to a highly active electrolyte, thus reducing the exothermic reaction. The measured powders were collected and their structures were characterized by XRD (Fig. 6(b)). After the DSC analysis up to 350 ℃, the structure of the delithiated materials were considerably destroyed. In the case of bare sample, MnF_2 and LiF peaks were observed. In contrast, the patterns of 2LCP sample showed much smaller impurity peaks than those of bare. When oxygen was released during the DSC measurements, the Li and Mn ions, which were extricated from the oxygen framework, reacted with the F ions from the

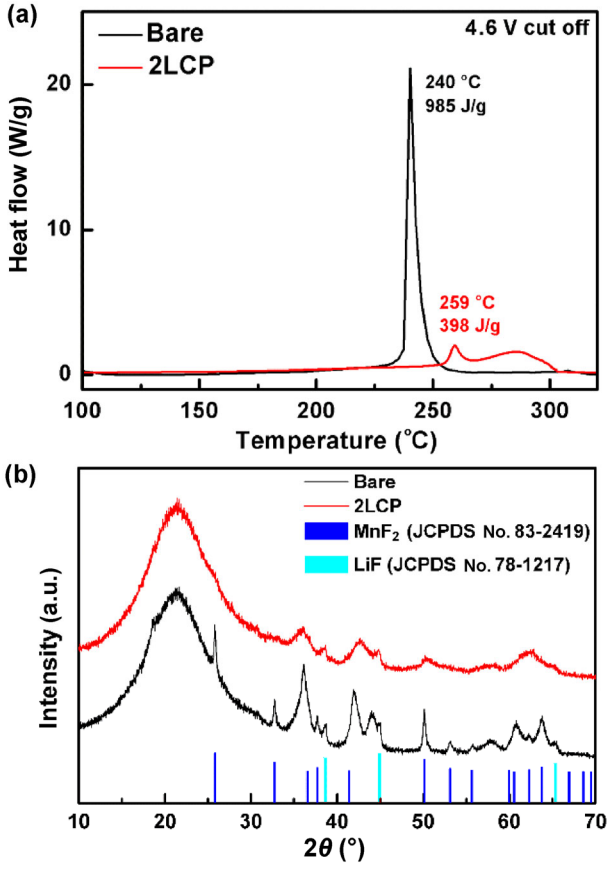

Figure 6 (a) DSC of bare and 2LCP at 4.6 V. (b) *Ex-situ* XRD patterns of samples; powders after DSC measurement from 50 to 350 ˚C.

lithium salt ($LiPF_6$), resulting in the formation of MnF_2 and LiF. These results reveal that the double protection layers effectively reduced the contact area between the surface of 2LCP and electrolyte, which contributed to the cycling and thermal stabilities.

4 Conclusions

In summary, we successfully synthesized $LiCoPO_4$ coated $0.4Li_{2-x}MnO_3$-$0.6LiNi_{1/3}Co_{1/3}Mn_{1/3}O_2$ material using the dual functioned coating method, without the formation of lithium impurities. The chemical activation and surface coating with $LiCoPO_4$ were carried out simultaneously. From the STEM and EDX analyses, spinel structure with higher Co and lower Mn content than the inner part was observed on the surface of the host particles, and the concentration of Co was found to decrease gradually towards the inward direction. The presence of spinel on the surface provided the facile pathway for lithium, leading to the superior rate capability. The double protective layers, $LiCoPO_4$ and cation-doped spinel, not only effectively suppressed the side reactions resulting in improved cycling performances, especially at 60 ˚C, but also protected the highly oxidized cathode materials from coming in direct contact with the electrolyte, leading to superior thermal stability. In addition, the spinel structure on the surface might hinder the transition metal ions from migrating to the lithium layers. Consequently, the simultaneous surface modification method of chemical activation and surface coating was found to be a simple and efficient strategy to enhance the electrochemical and thermal properties. We believe that this concept could contribute to the progress of the industry and research area. Since the voltage decay originates from the change in bulk structure as well as surface structure during cycling, fundamental researches on the bulk structure is necessary to prevent voltage decay completely.

Acknowledgements

This work was supported by the IT R&D program of MOTIE/KEIT (Development of Li-rich Cathode and Carbon-free Anode Materials for High Capacity/High Rate Lithium secondary Batteries, No. 10046309).

Electronic Supplementary Material: Supplementary material (SEM images and EDX date of bare and 2LCP, voltage profiles of bare and 2LCP upon cycling at 24 and 60 ˚C. XRD data, and C 1s XPS spectra of bare and 2LCP for analyzing Li_2CO_3) is available in the online version of this article at https://doi.org/10.1007/s12274-017-1662-8.

References

[1] Choi, N. S.; Chen, Z. H.; Freunberger, S. A.; Ji, X. L.; Sun, Y. K.; Amine, K.; Yushin, G.; Nazar, L. F.; Cho, J.; Bruce, P. G. Challenges facing lithium batteries and electrical double-layer capacitors. *Angew. Chem., Int. Ed.* **2012**, *51*, 9994–10024.

[2] Dunn, B.; Kamath, H.; Tarascon, J. M. Electrical energy storage for the grid: A battery of choices. *Science* **2011**, *334*, 928–935.

[3] Thackeray, M. M.; Wolverton, C.; Isaacs, E. D. Electrical energy storage for transportation-approaching the limits of, and going beyond, lithium-ion batteries. *Energy Environ. Sci.* **2012**, *5*, 7854–7863.

[4] Sun, Y. K.; Lee, M. J.; Yoon, C. S.; Hassoun, J.; Amine, K.; Scrosati, B. The role of AlF3 coatings in improving electrochemical cycling of Li-enriched nickel-manganese oxide electrodes for Li-ion batteries. *Adv. Mat.* **2012**, *24*, 1192–1196.

[5] Gu, M.; Belharouak, I.; Genc, A.; Wang, Z. G.; Wang, D. P.; Amine, K.; Gao, F.; Zhou, G. W.; Thevuthasan, S.; Baer, D. R. et al. Conflicting roles of nickel in controlling cathode performance in lithium ion batteries. *Nano Lett.* **2012**, *12*, 5186–5191.

[6] Yu, H. J.; Ishikawa, R.; So, Y. G.; Shibata, N.; Kudo, T.; Zhou, H. S.; Ikuhara, Y. Direct atomic-resolution observation of two phases in the $Li_{1.2}Mn_{0.567}Ni_{0.166}Co_{0.067}O_2$ cathode material for lithium-ion batteries. *Angew. Chem., Int. Ed.* **2013**, *52*, 5969–5973.

[7] Makimura, Y.; Ohzuku, T. Lithium insertion material of $LiNi_{1/2}Mn_{1/2}O_2$ for advanced lithium-ion batteries. *J. Power Sources* **2003**, *119–121*, 156–160.

[8] Sun, Y. K.; Myung, S. T.; Park, B. C.; Prakash, J.; Belharouak, I.; Amine, K. High-energy cathode material for long-life and safe lithium batteries. *Nat. Mater.* **2009**, *8*, 320–324.

[9] Cho, Y.; Oh, P.; Cho, J. A new type of protective surface layer for high-capacity Ni-based cathode materials: Nanoscaled surface pillaring layer. *Nano Lett.* **2013**, *13*, 1145–1152.

[10] Wu, C. R.; Fang, X. P.; Guo, X. W.; Mao, Y.; Ma, J.; Zhao, C. C.; Wang, Z. X.; Chen, L. Q. Surface modification of $Li_{1.2}Mn_{0.54}Co_{0.13}Ni_{0.13}O_2$ with conducting polypyrrole. *J. Power Sources* **2013**, *231*, 44–49.

[11] Yabuuchi, N.; Lu, Y. C.; Mansour, A. N.; Chen, S.; Shao-Horn, Y. The influence of heat-treatment temperature on the cation distribution of $LiNi_{0.5}Mn_{0.5}O_2$ and its rate capability in lithium rechargeable batteries. *J. Electrochem. Soc.* **2011**, *158*, A192–A200.

[12] Croy, J. R.; Kim, D.; Balasubramanian, M.; Gallagher, K.; Kang, S. H.; Thackeray, M. M. Countering the voltage decay in high capacity $xLi_2MnO_3{\cdot}(1-x)LiMO_2$ electrodes (M = Mn, Ni, Co) for Li^+-ion batteries. *J. Electrochem. Soc.* **2012**, *159*, A781–A790.

[13] Wang, J.; Yuan, G. X.; Zhang, M. H.; Qiu, B.; Xia, Y. G.; Liu, Z. P. The structure, morphology, and electrochemical properties of $Li_{1+x}Ni_{1/6}Co_{1/6}Mn_{4/6}O_{2.25+x/2}$ ($0.1 \le x \le 0.7$) cathode materials. *Electrochim. Acta* **2012**, *66*, 61–66.

[14] Jung, Y. S.; Cavanagh, A. S.; Yan, Y. F.; George, S. M.; Manthiram, A. Effects of atomic layer deposition of Al_2O_3 on the $Li[Li_{0.20}Mn_{0.54}Ni_{0.13}Co_{0.13}]O_2$ cathode for lithium-ion batteries. *J. Electrochem. Soc.* **2011**, *158*, A1298–A1302.

[15] Park, M. S.; Lee, J. W.; Choi, W.; Im, D.; Doo, S. G.; Park, K. S. On the surface modifications of high-voltage oxide cathodes for lithium-ion batteries: New insight and significant safety improvement. *J. Mater. Chem.* **2010**, *20*, 7208–7213.

[16] Zhang, X. F.; Belharouak, I.; Li, L.; Lei, Y.; Elam, J. W.; Nie, A. M.; Chen, X. Q.; Yassar, R. S.; Axelbaum, R. L. Structural and electrochemical study of Al_2O_3 and TiO_2 coated $Li_{1.2}Ni_{0.13}Mn_{0.54}Co_{0.13}O_2$ cathode material using ALD. *Adv. Energy Mater.* **2013**, *3*, 1299–1307.

[17] Kang, S. H.; Thackeray, M. M. Enhancing the rate capability of high capacity $xLi_2MnO_3{\cdot}(1-x)LiMO_2$ (M = Mn, Ni, Co) electrodes by Li-Ni-PO_4 treatment. *Electrochem. Commun.* **2009**, *11*, 748–751.

[18] Qiao, Q. Q.; Zhang, H. Z.; Li, G. R.; Ye, S. H.; Wang, C. W.; Gao, X. P. Surface modification of Li-rich layered $Li(Li_{0.17}Ni_{0.25}Mn_{0.58})O_2$ oxide with Li-Mn-PO_4 as the cathode for lithium-ion batteries. *J. Mater. Chem. A* **2013**, *1*, 5262–5268.

[19] Kang, S. H.; Johnson, C. S.; Vaughey, J. T.; Amine, K.; Thackeray, M. M. The effects of acid treatment on the electrochemical properties of $0.5Li_2MnO_3{\cdot}0.5LiNi_{0.44}Co_{0.25}Mn_{0.31}O_2$ electrodes in lithium cells. *J. Electrochem. Soc.* **2006**, *153*, A1186–A1192.

[20] Xu, G. F.; Li, J. L.; Xue, Q. R.; Ren, X. P.; Yan, G.; Wang, X. D.; Kang, F. Y. Enhanced oxygen reducibility of $0.5Li_2MnO_3{\cdot}0.5LiNi_{1/3}Co_{1/3}Mn_{1/3}O_2$ cathode material with mild acid treatment. *J. Power Sources* **2014**, *248*, 894–899.

[21] Kim, J. S.; Johnson, C. S.; Vaughey, J. T.; Thackeray, M. M. Pre-conditioned layered electrodes for lithium batteries. *J. Power Sources* **2006**, *153*, 258–264.

[22] Oh, P.; Ko, M.; Myeong, S.; Kim, Y.; Cho, J. A novel surface treatment method and new insight into discharge voltage deterioration for high-performance $0.4Li_2MnO_3$–$0.6LiNi_{1/3}Co_{1/3}Mn_{1/3}O_2$ cathode materials. *Adv. Energy Mater.* **2014**, *4*, 1400631, DOI: 10.1002/aenm.201400631.

[23] Oh, P.; Myeong, S.; Cho, W.; Lee, M. J.; Ko, M.; Jeong, H. Y.; Cho, J. Superior long-term energy retention and volumetric energy density for Li-rich cathode materials. *Nano Lett.* **2014**, *14*, 5965–5972.

[24] Wu, F.; Li, N.; Su, Y. F.; Zhang, L. J.; Bao, L. Y.; Wang, J.; Chen, L.; Zheng, Y.; Dai, L. Q.; Peng, J. Y. et al. Ultrathin spinel membrane-encapsulated layered lithium-rich cathode material for advanced Li-ion batteries. *Nano Lett.* **2014**, *14*, 3550–3555.

[25] Gu, M.; Genc, A.; Belharouak, I.; Wang, D. P.; Amine, K.; Thevuthasan, S.; Baer, D. R.; Zhang, J. G.; Browning, N. D.; Liu, J. et al. Nanoscale phase separation, cation ordering, and surface chemistry in pristine $Li_{1.2}Ni_{0.2}Mn_{0.6}O_2$ for Li-ion batteries. *Chem. Mater.* **2013**, *25*, 2319–2326.

[26] Zheng, J. M.; Gu, M.; Genc, A.; Xiao, J.; Xu, P. H.; Chen, X. L.; Zhu, Z. H.; Zhao, W. B.; Pullan, L.; Wang, C. M. et al. Mitigating voltage fade in cathode materials by improving the atomic level uniformity of elemental distribution. *Nano Lett.* **2014**, *14*, 2628–2635.

[27] Kim, Y.; Cho, J. Lithium-reactive $Co_3(PO_4)_2$ nanoparticle coating on high-capacity $LiNi_{0.8}Co_{0.16}Al_{0.04}O_2$ cathode material for lithium rechargeable batteries. *J. Electrochem. Soc.* **2007**, *154*, A495–A499.

[28] Park, M. H.; Noh, M.; Lee, S.; Ko, M.; Chae, S.; Sim, S.; Choi, S.; Kim, H.; Nam, H.; Park, S. et al. Flexible high-energy Li-ion batteries with fast-charging capability. *Nano Lett.* **2014**, *14*, 4083–4089.

[29] Lee, M. J.; Lee, S.; Oh, P.; Kim, Y.; Cho, J. High performance $LiMn_2O_4$ cathode materials grown with epitaxial layered nanostructure for Li-ion batteries. *Nano Lett.* **2014**, *14*, 993–999.

[30] Huang, R.; Ikuhara, Y. H.; Mizoguchi, T.; Findlay, S. D.; Kuwabara, A.; Fisher, C. A. J.; Moriwake, H.; Oki, H.; Hirayama, T.; Ikuhara, Y. Oxygen-vacancy ordering at surfaces of lithium manganese(III, IV) oxide spinel nanoparticles. *Angew. Chem., Int. Ed.* **2011**, *50*, 3053–3057.

[31] Thackeray, M. M.; Kang, S. H.; Johnson, C. S.; Vaughey, J. T.; Benedek, R.; Hackney, S. A. Li_2MnO_3-stabilized $LiMO_2$ (M = Mn, Ni, Co) electrodes for lithium-ion batteries. *J. Mater. Chem.* **2007**, *17*, 3112–3125.

[32] Johnson, C. S.; Li, N.; Vaughey, J. T.; Hackney, S. A.; Thackeray, M. M. Lithium-manganese oxide electrodes with layered-spinel composite structures $xLi_2MnO_3\cdot(1-x)Li_{1+y}Mn_{2-y}O_4$ ($0 < x < 1$, $0 \le y \le 0.33$) for lithium batteries. *Electrochem. Commun.* **2005**, *7*, 528–536.

[33] Wu, F.; Li, N.; Su, Y. F.; Shou, H. F.; Bao, L. Y.; Yang, W.; Zhang, L. J.; An, R.; Chen, S. Spinel/layered heterostructured cathode material for high-capacity and high-rate Li-ion batteries. *Adv. Mat.* **2013**, *25*, 3722–3726.

[34] Ohzuku, T.; Takeda, S.; Iwanaga, M. Solid-state redox potentials for $Li[Me_{1/2}Mn_{3/2}]O_4$ (Me: 3d-transition metal) having spinel-framework structures: A series of 5 volt materials for advanced lithium-ion batteries. *J. Power Sources* **1999**, *81–82*, 90–94.

[35] Kim, J. H.; Myung, S. T.; Yoon, C. S.; Kang, S. G.; Sun, Y. K. Comparative study of $LiNi_{0.5}Mn_{1.5}O_{4-\delta}$ and $LiNi_{0.5}Mn_{1.5}O_4$ cathodes having two crystallographic structures: $Fd\bar{3}m$ and $P4_332$. *Chem. Mater.* **2004**, *16*, 906–914.

[36] Han, D. W.; Kang, Y. M.; Yin, R. Z.; Song, M. S.; Kwon, H. S. Effects of Fe doping on the electrochemical performance of $LiCoPO_4$/C composites for high power-density cathode materials. *Electrochem. Commun.* **2009**, *11*, 137–140.

[37] Rui, X. H.; Zhao, X. X.; Lu, Z. Y.; Tan, H. T.; Sim, D.; Hng, H. H.; Yazami, R.; Lim, T. M.; Yan, Q. Y. Olivine-type nanosheets for lithium ion battery cathodes. *ACS Nano* **2013**, *7*, 5637–5646.